Molecular spin in a fluid undergoing Poiseuille flow

Karl P. Travis and D. J. Evans

Research School of Chemistry, Australian National University, G.P.O. Box 414, Canberra, Australian Capital Territory 2601, Australia

We use nonequilibrium molecular dynamics to investigate shear induced molecular rotation in a diatomic fluid undergoing planar Poiseuille flow. We have compared the angular velocity and translational streaming velocity profiles with the predictions of Navier-Stokes hydrodynamics generalized for systems that possess spin. We find that the angular velocity profile is in general agreement with the profile predicted from the Navier-Stokes theory except for some features close to the walls which are likely to be a result of molecular packing. [S1063-651X(97)00102-5]

PACS number(s): 03.40.Gc, 02.50.−r, 51.10.+y, 05.70.Ln

I. INTRODUCTION

Classical Navier-Stokes theory strictly applies only to simple fluids composed of inert gas atoms. This is because Navier-Stokes hydrodynamics takes no account of the structure or the possible alignment of the particles comprising a fluid. The most well developed extension of Navier-Stokes hydrodynamics, which is capable of describing the flow of fluids composed of structured particles, is the theory which describes the flow of nematic liquid crystals [1–3]. This nemato dynamics treats the constituent molecules as rigid bodies and, in its most common form, the theory assumes the nematic order parameter is a constant of the motion. These two assumptions greatly simplify the theory. The most complex molecular fluids are those in which the nonequilibrium nematic order parameter is not constant and where the constituent molecules are relatively flexible, allowing shear induced changes to the internal conformation.

In this paper we will deal with the generalized hydrodynamics of fluids whose order parameter is not constant but whose constituent molecules can be regarded as classical rigid bodies. The hydrodynamics of such fluids was developed first by Grad [4] and then later by Snider and Lewchuk [5]. The resulting generalized Navier-Stokes equations have the advantage that for certain idealized flows, such as the planar Couette and Poiseuille flow, the solutions are analytic and therefore amenable to testing by computer simulation experiments.

Recently, there has been great interest in studying the flow of fluids through solid pores using nonequilibrium molecular dynamics. Most of these simulations have concerned simple fluids, i.e., those composed of structureless particles [6–15]. While some simulations of molecular fluids have been carried out [16–18], the microrotation or spin of the molecules has been overlooked.

In this article we perform simulations of a liquid composed of rigid diatomic molecules undergoing planar Poiseuille flow. We analyze the resulting translational velocity, and angular velocity profiles and compare them with the predictions of generalized Navier-Stokes theory for fluids which possess spin.

The Navier-Stokes equations appropriate for fluids composed of uniaxial molecules close to equilibrium are [19]

$$\rho \frac{d\mathbf{u}}{dt} = -\boldsymbol{\nabla}(p) + (\kappa + \eta/3 - \eta_r)\boldsymbol{\nabla}(\boldsymbol{\nabla}\cdot\mathbf{u}) + (\eta + \eta_r)\nabla^2\mathbf{u}$$
$$+ 2\eta_r(\boldsymbol{\nabla}\times\boldsymbol{\omega}), \tag{1}$$

$$\rho\Theta \frac{d\boldsymbol{\omega}}{dt} = 2\eta_r(\boldsymbol{\nabla}\times\mathbf{u} - 2\boldsymbol{\omega}) + (\zeta_v + \zeta/3 - \zeta_{rr})\boldsymbol{\nabla}(\boldsymbol{\nabla}\cdot\boldsymbol{\omega})$$
$$+ (\zeta + \zeta_{rr})\nabla^2\boldsymbol{\omega}, \tag{2}$$

where ρ is the mass density of the fluid, p the hydrostatic pressure, κ, η, η_r, the bulk, shear and vortex viscosities, respectively, $\zeta_v, \zeta, \zeta_{rr}$, the respective couple viscosities, and $\mathbf{u}$ is the streaming velocity. $\Theta \equiv \text{tr}\langle\boldsymbol{\Theta}_i\rangle/3 = \text{tr}(\boldsymbol{\Theta})/3$ is one third of the trace of the average moment of inertia tensor per unit mass and $\boldsymbol{\omega}$ is the streaming angular velocity. If $\mathbf{S}$ is the average intrinsic angular momentum per unit mass and $\boldsymbol{\omega}_i$ the angular velocity of molecule i, then

$$S = \langle\boldsymbol{\Theta}_i\cdot\boldsymbol{\omega}_i\rangle = \boldsymbol{\Theta}\cdot\boldsymbol{\omega}, \tag{3}$$

where

$$\boldsymbol{\Theta}_i = \sum_{\alpha \in i} m(r'^2_{i\alpha}\mathbf{1} - \mathbf{r}'_{i\alpha}\mathbf{r}'_{i\alpha}) \bigg/ \sum_{\alpha \in 1} m$$
$$= \sum_{\alpha \in i} m(r'^2_{i\alpha}\mathbf{1} - \mathbf{r}'_{i\alpha}\mathbf{r}'_{i\alpha}) \bigg/ M \tag{4}$$

is the moment of inertia tensor per unit mass of molecule i. The index α labels the atoms in molecule i and $\mathbf{r}'_{i\alpha}$ is the vector from the center of mass of molecule i to site α of the same molecule. These atoms are assumed here to have identical masses, namely, m. M is the total mass of molecule i.

In this paper we confine ourselves to uniaxial molecules (such as the halogens). For such molecules the principle moment of inertia tensor per unit mass of each molecule can be written as

$$\boldsymbol{\Theta}_{pi} = \begin{pmatrix} I & 0 & 0 \\ 0 & I & 0 \\ 0 & 0 & 0 \end{pmatrix}. \tag{5}$$

The equations of linear and intrinsic angular momentum written above only apply in the linear regime close to equi-

librium. This is because those equations assume the transport coefficients are independent of the driving thermodynamic forces and they neglect the higher order effects of shear bi-refringence on the intrinsic angular momentum equation. It is this linearity assumption that enables us to write $\mathbf{\Theta} \cdot \boldsymbol{\omega} = \Theta \boldsymbol{\omega}$.

We should also mention that even in the linear regime there is a difference for isotropic fluids between the streaming angular velocity and the average angular velocity, $\bar{\boldsymbol{\omega}}$. Since $I\bar{\boldsymbol{\omega}} = \Theta \boldsymbol{\omega}$, and $\Theta = \mathrm{tr} \langle \mathbf{\Theta}_{pi} \rangle / 3 = 2I/3$, we see that

$$\bar{\boldsymbol{\omega}} = 2\,\boldsymbol{\omega}/3. \tag{6}$$

We also note that Sarman and Evans [3] have proved that away from boundaries, in the absence of external applied torques, $\boldsymbol{\omega} = 1/2 \boldsymbol{\nabla} \times \mathbf{u}$. This relation holds for the streaming angular velocity but obviously *not* for the average angular velocity.

For a fluid flowing under the influence of a pressure gradient in the x direction (planar Poiseuille flow) between two infinite parallel plates a distance h apart whose normals are in the y direction, Eqs. (1) and (2) can be solved for the streaming linear and angular velocities [17]

$$u_x = u_c \left[1 - \bar{y}^2 + \frac{2\,\eta_r}{(\eta + \eta_r)Kh} \coth(Kh) \left(\frac{\cosh(Kh\bar{y})}{\cosh(Kh)} - 1 \right) \right], \tag{7}$$

$$\omega_z = \frac{u_c}{h} \left(\bar{y} - \frac{\sinh(Kh\bar{y})}{\sinh(Kh)} \right), \tag{8}$$

where $\bar{y} = y/h$,

$$K = \left[\frac{4\,\eta\,\eta_r}{(\eta + \eta_r)(\zeta + \zeta_{rr})} \right]^{1/2} \tag{9}$$

and

$$u_c = -\frac{h^2}{2\,\eta} \frac{dp}{dx}. \tag{10}$$

In deriving Eqs. (7) and (8) the assumptions that $\boldsymbol{\omega} = (0,0,\omega_z(y))$ and $\mathbf{u} = (u_x(y),0,0)$ (i.e., $\boldsymbol{\nabla} \cdot \boldsymbol{\omega} = 0$ and $\boldsymbol{\nabla} \cdot \mathbf{u} = 0$) have been used.

II. SIMULATION DETAILS

In this work we use nonequilibrium molecular dynamics to simulate a fluid composed of rigid diatomic molecules undergoing planar Poiseuille flow between two atomistic walls. Our method is essentially that used by Todd and co-workers [13–15] to study a simple fluid undergoing Poiseuille flow.

The geometry of the system is shown in Fig. 1. The system is surrounded by periodic images of itself in each of the three Cartesian dimensions. We note here that the simulation geometry is such that the driving pressure head is in the x direction and heat will flow in the y direction only. The pore width W is defined as the separation in the y direction between the centers of the first layer of wall atoms adjacent to the fluid. Our system consists of 360 fluid molecules bound by 216 wall atoms which were three atomic layers thick (72 atoms per layer).
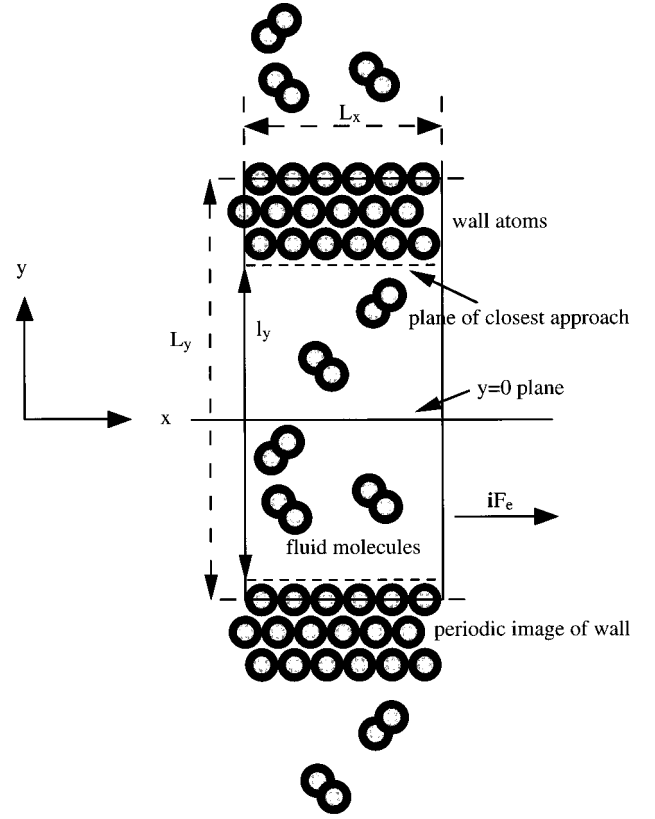
FIG. 1. Simulation geometry for planar Poiseuille flow. The z axis is normal to the plane.

Both the fluid atomic sites and wall atoms interact via the WCA interatomic potential function $\phi(r)$: $\phi(r) = 4(r^{-12} - r^{-6}) + 1$, for $r < 2^{1/6}$; $\phi(r) = 0$, for $r > 2^{1/6}$. We defined the Weeks, Chandler, Anderson (WCA) potential parameters σ and ϵ to be unity for simplicity; we also defined the site mass m to be unity, thus the molecule mass, $M = 2m$. These definitions define our reduced system of units.

The wall atoms were fixed in an fcc lattice structure by harmonic restoring forces [13]

$$\mathbf{\Phi}_{\mathrm{Harm}} = \tfrac{1}{2} K_s (\mathbf{r}_i - \mathbf{r}_i^{\mathrm{eq}})^2, \tag{11}$$

where K_s is the spring constant (which we take as 150.15) and $\mathbf{r}_i^{\mathrm{eq}}$ is the equilibrium position of a wall atom i. Wall layers are prevented from moving by a constraint mechanism which fixes the center of mass of each layer of wall particles while allowing individual wall atoms the freedom to vibrate about their lattice sites. There is only one three atom thick wall per simulation cell. The second wall is simply the periodic image of the first wall. This periodicity ensures that the total density of the system remains constant.

The equations of motion for the wall atoms are

$$\dot{\mathbf{r}}_i = \frac{\mathbf{p}_i}{m}, \tag{12}$$

$$\dot{\mathbf{p}}_i = \mathbf{F}_i^{\mathrm{Harm}} + \mathbf{F}_i^{\mathrm{WCA}} - \alpha \mathbf{p}_i - \mathbf{j}\lambda_k, \quad i \in L_k(k=1,2,3) \tag{13}$$

where $\mathbf{p}_i$ is the momentum of wall atom i, $\dot{\mathbf{r}}_i$ its velocity, m is the mass of a wall atom, $\mathbf{F}_i^{\text{Harm}}$ the harmonic restoring force on wall atom i, $\mathbf{F}_i^{\text{WCA}}$ the total intermolecular force on wall atom i due to all other wall atoms and all fluid molecular sites, α is a thermostatting multiplier, $\mathbf{j}$ is a unit vector along the laboratory fixed y-Cartesian axis, λ_k is the wall center-of-mass constraint multiplier for wall layer k. The form of Eq. (13) has been derived using Gauss's principle of least constraint [20]. Expressions for the thermostatting multiplier α, and the wall layer constraint multipliers λ_k, can be obtained by a second application of Gauss's principle of least constraint

$$\alpha = \frac{N_w \sum_{j}^{3N_w} \mathbf{F}_j \cdot \mathbf{p}_j - \sum_{k}^{3} F_k^y p_k^y}{N_w \sum_{j}^{3N_w} \mathbf{p}_j \cdot \mathbf{p}_j - \sum_{k}^{3} p_k^y p_k^y}, \tag{14}$$

$$\lambda_k = \frac{1}{N_w}\left[\sum_{i \in L_k}^{N_w} F_i^y - \alpha \sum_{i \in L_k}^{N_w} \mathbf{p}_i^y \right], \quad k=1,2,3 \tag{15}$$

where N_w is the number of wall atoms in a wall layer,

$$F_k^y = \mathbf{j} \cdot \sum_{i \in L_k}^{N_w} \mathbf{F}_i, \quad \text{and} \quad p_k^y = \mathbf{j} \cdot \sum_{i \in L_k}^{N_w} \mathbf{p}_i,$$

L_k is wall layer k. In the above equations, $\mathbf{F}_i$ now represents the sum of harmonic and intermolecular forces. While the Gaussian algorithm is formally exact, in very long simulation runs truncation and discretization errors lead to a slow drift in the values of the constrained variables. To counter this, we have used a continuous linear proportional feedback mechanism. One simply adds the following terms to the equations of motion for the wall atoms. For the temperature feedback we add the term

$$-B[T_w(t) - T_w]\mathbf{p}_i, \tag{16}$$

where $T_w(t)$ is the instantaneous wall temperature, T_w is the required wall temperature, and B is a constant. In these simulations we have taken $B=100$. For the feedback on the wall center-of-mass positions we add the following terms to Eqs. (12) and (13), respectively:

$$-\frac{C}{N_w}\left[\sum_{i \in L_k}^{N_w} y_i - \sum_{i \in L_k}^{N_w} y_i(t=0) \right], \quad k=1,2,3 \tag{17}$$

$$-\frac{D}{N_w} \sum_{i \in L_k}^{N_w} \dot{y}_i, \quad k=1,2,3. \tag{18}$$

In the above expressions, C and D are feedback constants. In these simulations we haven taken the values $C=10$ and $D=0$.

In our simulations there are no pressure gradients. Instead we apply a constant external field which has the effect of applying a constant force in the x direction to each molecular center of mass. In computer simulations, the advantage of using an external field to drive the flow rather than an actual pressure gradient is that under a constant external field the

system can remain longitudinally homogeneous. Under an actual pressure gradient this is not possible because in compressible fluids, pressure gradients imply density gradients. The equations of motion for a site α in fluid molecule i are

$$\dot{\mathbf{r}}_{i\alpha} = \frac{\mathbf{p}_{i\alpha}}{m}, \tag{19}$$

$$\dot{\mathbf{p}}_{i\alpha} = \mathbf{F}_{i\alpha}^{\text{WCA}} + (-1)^\alpha \lambda_i \mathbf{r}_{i12} + \frac{1}{2}\,\mathbf{i}F_e, \tag{20}$$

where the mass of molecular sites is taken to be the same as the mass of the wall particles, $\mathbf{i}$ is a unit vector along the laboratory fixed x-Cartesian axis and F_e is the magnitude of the externally applied field. In Eq. (20), λ_i is a Gaussian bond constraint multiplier and $\mathbf{r}_{i12}$ is defined by $\mathbf{r}_{i2} - \mathbf{r}_{i1}$. An expression for λ_i is obtained by an application of Gauss's principle of least constraint

$$\lambda_i = -\frac{[\mathbf{r}_{i12} \cdot \mathbf{F}_{i\alpha}^{\text{WCA}} + m(\dot{\mathbf{r}}_{i12})^2]}{2(\mathbf{r}_{i12})^2}. \tag{21}$$

Linear proportional feedback needs to be introduced to counter any drift in the bond lengths and component of velocity down the bond. This is achieved by adding the following terms to Eqs. (19) and (20), respectively,

$$-F(r_{i12} - d_{12})\hat{\mathbf{r}}_{i12}, \tag{22}$$

$$-G(\dot{\mathbf{r}}_{i12} \cdot \hat{\mathbf{r}}_{i12})\hat{\mathbf{r}}_{i12}, \tag{23}$$

where r_{i12} is the magnitude of the bond vector in molecule i, d_{12} is the required bond length, $\hat{\mathbf{r}}_{i12}$ is a unit vector in the direction of the bond, and $\dot{\mathbf{r}}_{i12}$ is the bond velocity. Values for the drift constants F and G used in this work are 10 and 15, respectively.

The walls were kept at a constant temperature of 0.971 and a number density of 0.90. With this choice for the wall density and our choice of harmonic force constant, we found that no molecules were able to penetrate into the wall layers. Lowering the force constant to the value suggested by Liem, Brown, and Clarke [11], i.e., $K_s = 57.15$, results in significant penetration of the walls by fluid molecules, though this value of K_s would facilitate the coupling of heat exchange between the walls and the fluid. The number density of the fluid was $n = N/V = 0.544$ at the start of the simulation where N is the number of liquid atoms and V is the volume accessible to the liquid. The reduced pore width is 10.2 while the unit cell dimensions, L_x, L_y, L_z, are 8.481, 9.200, 8.481. It is important to note that L_y includes the fluid and wall particles (see Fig. 1). We observe that there is no clear definition of the average density of the fluid because there is no unambiguous definition of the total volume which is ''accessible'' to the fluid, and again refer the reader to Refs. [13] and [14] for a discussion of this. We simply note here that an effective pore width was found to be $L_y = 9.0$.

The equations of motion were integrated using a fourth-order Gear predictor-corrector algorithm with a reduced time step, $\tau = 0.001$. Our initial configuration was constructed as follows: Having constructed a wall layer (72 atoms arranged in an fcc lattice) this was replicated and shifted to construct the three layer wall composed of 216 atoms. One of the wall

layers was then replicated a further five times to form five fluid layers of atoms equally spaced throughout the remainder of the simulation cell. The coordinates of these fluid sites were then taken to be the positions of the centers of mass of the fluid *molecules*. The molecules were then constructed using the known geometry of the diatomics (all molecules are constructed with the same orientation for simplicity). Of course, starting the simulation from this point would result in difficulties because large forces would result from particle overlap. To circumvent this problem, we use the truncated force method (TFM) of McKecknie, Brown, and Clarke [21]. Using this method, we find that the configuration was sufficiently relaxed after only a few thousand time steps to enable the full WCA potential to be switched on. The system was then allowed to come to equilibrium in the absence of an external field. Typically, we use between half and one million steps to achieve equilibrium since the fluid temperature is a slowly relaxing quantity. Nonequilibrium molecular dynamics (NEMD) simulations were then performed by first equilibrating for a million time steps with the field switched on followed by 2 million step production runs. We studied the system at two different values of the magnitude of the external field, $F_e = 0.2$ and 0.5.

Determination of the translational and angular velocity profiles

The streaming velocity can be obtained from the instantaneous momentum current density, $\mathbf{J}(\mathbf{r},t)$. The momentum current density for a system of identical particles is given microscopically by [20]

$$\mathbf{J}(\mathbf{r},t) \equiv \rho \mathbf{u}(\mathbf{r},t) = \sum_i M \mathbf{v}_i \delta(\mathbf{r} - \mathbf{r}_i(t)), \qquad (24)$$

where the instantaneous mass density, $\rho(\mathbf{r},t)$ is given by

$$\rho(\mathbf{r},t) = \sum_i M \delta(\mathbf{r} - r_i(t)) \equiv M n(\mathbf{r},t), \qquad (25)$$

where $n(\mathbf{r},t)$ is the instantaneous number density at position $\mathbf{r}$ and time $\mathbf{t}$. The streaming velocity is then simply

$$\mathbf{u}(\mathbf{r},t) = \frac{\sum_i M \mathbf{v}_i(t) \delta(\mathbf{r} - \mathbf{r}_i(t))}{\sum_i M \delta(\mathbf{r} - \mathbf{r}_i(t))}. \qquad (26)$$

In practice, one replaces the Dirac δ function by a narrow step function that is nonzero only for a small range of separations. For a system such as ours we could divide the simulation cell into a number of slabs of thickness Δ_y and compute the streaming velocity as an average evaluated at the midpoint of each slab. This is the simple histogram method. While it is simple to use and implement, it suffers from the drawback that the slab width must be sufficiently large to contain enough particles to allow a good estimate of the average streaming velocity in a slab [11]. Thus there is a trade-off between lower statistical uncertainty and spatial resolution in the histogram method.

Recently, Daivis, Travis, and Todd [22] have proposed an alternative method of calculating microscopic quantities as a function of position which is exact. In this method one notionally divides the simulation cell into a number of equally spaced planes across the pore.

One can write for the density and the x component of momentum current

$$\rho(y,t) = \frac{1}{A} \sum_i M \delta(y - y_i(t)) \qquad (27)$$

and

$$J_x(y,t) = \frac{1}{A} \sum_i M \dot{x}_i(t) \delta(y - y_i(t)), \qquad (28)$$

where $A = L_x L_z$ is the area of an xz plane. If $\{t_{\alpha(i)}\}$ is the set of times when the y coordinate of particle i is equal to some specified value y, which defines a plane, one has that, $\delta(y - y_i(t_{\alpha(i)})) = \delta(t - t_{\alpha(i)})/|\dot{y}_i(t_{\alpha(i)})|$. Therefore we can obviously write

$$\delta(y - y_i(t)) = \sum_{t_{\alpha(i)}} \frac{\delta(t - t_{\alpha(i)})}{|\dot{y}_i(t_{\alpha(i)})|}. \qquad (29)$$

Substituting Eq. (29) into Eq. (28) we find that,

$$J_x(y,t) = \frac{1}{A} \sum_i \sum_{t_{\alpha(i)}} \frac{M \dot{x}_i(t) \delta(t - t_{\alpha(i)})}{|\dot{y}_i(t_{\alpha(i)})|}. \qquad (30)$$

Assuming the system properties are stationary in time we integrate Eq. (30) from time zero to τ and perform a time average

$$J_x(y) = \lim_{\tau \to \infty} \frac{1}{\tau A} \sum_i \sum_{0 < t_{\alpha(i)} < \tau} \frac{M \dot{x}_i(t_{\alpha(i)})}{|\dot{y}_i(t_{\alpha(i)})|}. \qquad (31)$$

Similarly, one can write for the mass density.

$$\rho(y) = \lim_{\tau \to \infty} \frac{1}{\tau A} \sum_i \sum_{0 < t_{\alpha(i)} < \tau} \frac{M_i}{|\dot{y}_i(t_{\alpha(i)})|}. \qquad (32)$$

The spin angular momentum density at position $\mathbf{r}$ is defined instantaneously as

$$\rho \mathbf{S}(\mathbf{r},t) = \sum_i \mathbf{s}_i \delta(\mathbf{r} - \mathbf{r}_i(t)) \equiv \sum_i \sum_\alpha \mathbf{r}'_{i\alpha} \times \mathbf{p}_{i\alpha} \delta(\mathbf{r} - \mathbf{r}_i(t)), \qquad (33)$$

where, $\mathbf{s}_i$ is the spin angular momentum of molecule i, $r'_{i\alpha} = \mathbf{r}_{i\alpha} - \mathbf{r}_i$. The angular streaming velocity, $\boldsymbol{\omega}$ is defined through the hydrodynamic expression [Eq. (3)]. For uniaxial molecules

$$\rho(y) S_z(y) = \lim_{\tau \to \infty} \frac{1}{\tau A} \sum_i \sum_{0 < t_{\alpha(i)} < \tau} \frac{s_{zi}(t_{\alpha(i)})}{|\dot{y}_i(t_{\alpha(i)})|}. \qquad (34)$$

One can now use Eqs. (3) and (34) to calculate $\omega_z(y)$. To obtain the spins at a plane, we calculate the relative positions and velocities at the time the *molecular center of mass crosses a plane* in the y direction.

The y component of the velocity or angular momentum of particle i at the precise time of the plane crossing is evaluated by first solving for $t_{\alpha(i)}$, the time at which plane y is
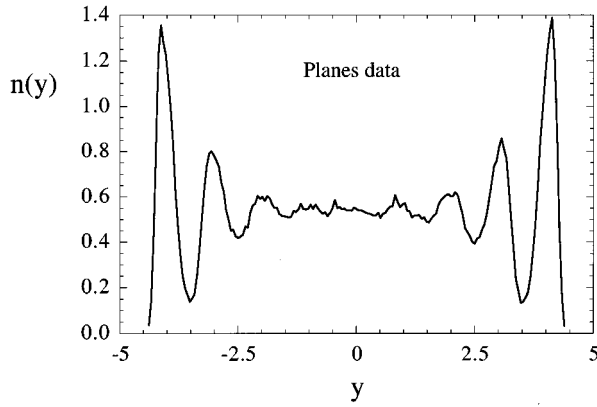
FIG. 2. Fluid number density profile for an external field magnitude $F_e = 0.2$. Statistical uncertainties are smaller than the plot symbols.

FIG. 3. Plot of the dimensionless quantity, $h\omega_z/u_c$ vs y/h for various values of the product Kh.

crossed, by using a Newton-Raphson scheme and then predicting the velocity of the atom at this time. It is straightforward to calculate the density and kinetic energy profiles using this method and, hence, the streaming velocity and kinetic temperature profiles. Using this method we are able to use a fine resolution in calculating the profiles. In this work we used 200 planes.

Another route to the angular velocity profile involves binning the molecular angular velocities at each time step. One then uses Eq. (6) to determine the average streaming angular velocity from the average angular velocity. This gives

$$\omega_z(y,t) = \frac{3}{2A} \sum_i \omega_{zi}(t)\,\delta(y - y_i(t)). \qquad (35)$$

Test simulations yielded agreement between profiles calculated by either of these methods although the binning method gave the better statistics. For this reason we choose to use the binning method for calculating the angular velocity profiles in this work.

III. RESULTS AND DISCUSSION

Number density

Figure 2 shows the mass density profile from the $F_e = 0.2$ simulation. We observe that the mass density falls to zero at $y = \pm 4.5$ which suggests an effective porewidth of 9.0. The mass density shows strong oscillations near the walls and shows evidence of the fluid forming eight layers in a porewidth of 10.2 molecular diameters wide. The profile is qualitatively the same as that obtained by Todd and Evans [15] for an atomic fluid confined to a channel of the same width.

Microrotation

To facilitate comparison of the simulation results with the Navier-Stokes theory, following Eringen [23], we rearrange Eq. (8) so that the left-hand side of this equation is now dimensionless and the right-hand side is solely a function of the dimensionless quantity, Kh:

$$\frac{h\omega_z}{u_c} = \bar{y} - \frac{\sinh(Kh\bar{y})}{\sinh(Kh)}. \qquad (36)$$

The classical Navier-Stokes result for angular velocity is trivially zero since no account is taken of microrotation in that theory. The inclusion of spin into the theory results in a form for the angular velocity which contains a linear term plus a hyperbolic term. In the absence of the hyperbolic term, the linear term would simply imply that the streaming angular velocity was half the vorticity. The hyperbolic term is basically a switch function which controls the rate at which the streaming angular velocity changes from its boundary value (namely, zero) towards its preferred value of half the vorticity.

For a constant value of u_c the theoretical variation of the streaming angular velocity with the dimensionless parameter Kh is shown in Fig. 3. At $Kh = 1$, the angular velocity profile is almost flat and close to zero. The hyperbolic switch is so broad that the midchannel angular velocity is never allowed to approach its preferred value of half the vorticity. As the value of Kh increases to ~ 10, the switch becomes sharper allowing the midchannel angular velocity to attain its preferred value. By the time $Kh \sim 100$ the preferred value for the angular velocity is attained across most of the channel and there is a very sharp transition of the angular velocity to zero at the boundaries.

Figure 4 shows a plot of the angular velocity as a function of the porewidth (the results are taken from the $F_e = 0.5$ simulation). The streaming angular velocity profile is similar
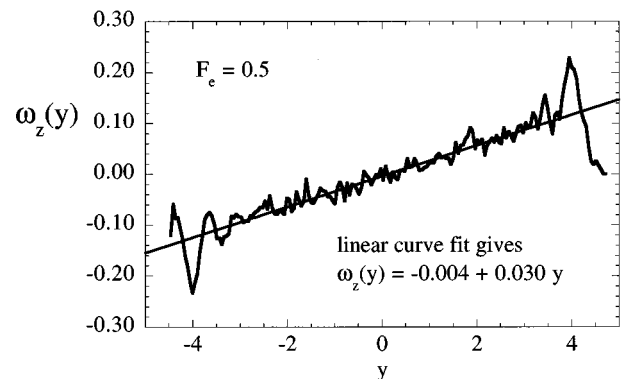
FIG. 4. Angular velocity profile for $F_e = 0.5$. The linear function is the result of a least squares fit to the data. The slope of this curve fit is equal to one half the vorticity.
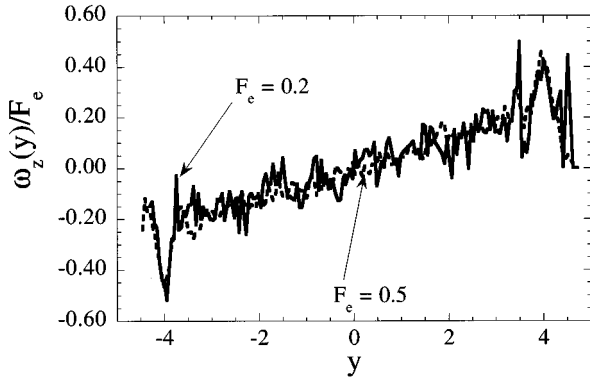
FIG. 5. Plot of the normalized angular velocity, ω_z/F_e. The solid line is data from the $F_e=0.2$ simulation while the dashed line is data from the $F_e=0.5$ simulation.

to the theoretical prediction with Kh between 10 and 100, as is shown in Fig. 3. The large peaks that appear around $y=\pm4$ in Fig. 4 are not accounted for in the theory but this is not surprising. The theory given above is a continuum theory which does not allow for molecular packing effects near the walls. The wavelength of the oscillations is σ so they are almost certainly due to packing effects which are not accounted for in the continuum theory presented in this paper. Applying a simple linear fit to the angular velocity data in Fig. 4 shows that in midchannel $\partial\omega_z/\partial y\sim0.030\pm0.001$. If instead, we use a nonlinear least squares procedure to fit the data to Eq. (8), for $F_e=0.5$ the results of the fit give $u_c=0.69\pm0.02$ and $Kh=20\pm3$, while for $F_e=0.2$, the results of the fit give $u_c=0.25\pm0.01$ and $Kh=32\pm14$. Two points can be made concerning these fit results. Firstly, the ratio of the two values of $u_c=2.76$ is very close to the ratio of the two external fields, suggesting a linear dependence on the magnitude of the external field or pressure gradient. Figure 5 shows a plot of the streaming angular velocity normalized by the magnitude of the external field for the two different sets of data corresponding to $F_e=0.2$ and $F_e=0.5$. The angular velocity profiles are superimposable, confirming the linear dependence upon the field strength.

Streaming velocity

Figure 6 shows the translational velocity profile for an
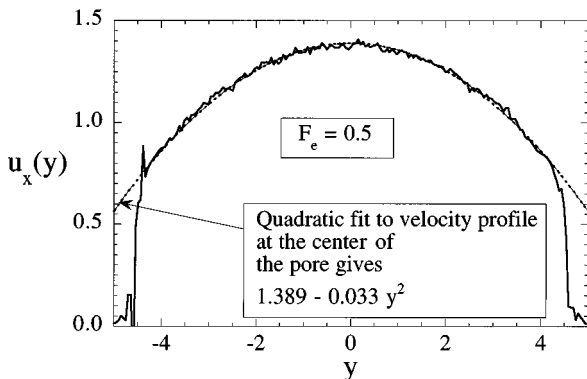
FIG. 6. Translational velocity profile at $F_e=0.5$ (solid line) and the least squares fit of the data in the center of the pore to a two parameter quadratic function (dotted line).
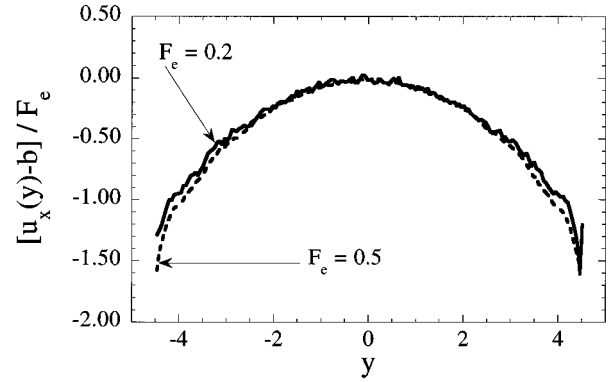
FIG. 7. Plot of the normalized translational streaming velocity, $(u_x-b)/F_e$. The solid line is data from the $F_e=0.2$ simulation while the dashed line is data from the $F_e=0.5$ simulation. The parameter b is the constant term obtained from the quadratic fit to the streaming velocity data.

external field, $F_e=0.5$. At the effective pore boundaries, $y=\pm4.5$, the velocity profile drops sharply to zero, indicating severe slip, while towards the central region of the pore, a quadratic behavior can be seen. The severity of the slip may be the result of having wall molecules which are different from the fluid molecules. We note that the quadratic portion of the velocity profile is still not classical because two parameters are required to fit the data whereas only one parameter is required in the classical case. The reason for this discrepancy is related to the boundary conditions. From the curve fit equation, we see that the vorticity, $\frac{1}{2}\nabla\times\mathbf{u}=0.033$. This agrees well with the slope of the linear portion of the angular streaming velocity shown in Fig. 4.

An attempt at a nonlinear least squares fit of Eq. (7) to the velocity data resulted in a very poor fit. However, from the form of Eq. (7) we see that if the vortex viscosity, η_r is small in comparison to the shear viscosity, η, the spin contribution to the translational streaming velocity is negligible and molecular spin plays no significant role in the transport of linear momentum. Edberg, Morriss, and Evans [24] obtained a value for the vortex viscosity of liquid chlorine at a reduced number density of 0.544 and a reduced translational temperature of 0.97 (conditions which are close to the mean number density and mean translational temperature at the center of our pore). Their value of $\eta_r(\gamma=0)=0.020\pm0.005$ is indeed small compared to the value they obtained for the shear viscosity; $\eta(\gamma=0)\approx5$.

We can calculate an effective shear viscosity from Eq. (10). Rearranging Eq. (10) gives

$$\eta=\frac{\bar{n}h^2F_e}{2u_c},\qquad(37)$$

where $\bar{n}$ is now the mean number density in our system. Because the number density profile oscillates strongly near the walls, we integrate the profile in the central region to obtain $\bar{n}=0.543$, which is close to the input density of $\bar{n}=0.544$ (the density of Edberg, Morriss, and Evans [24]). Putting the relevant values into Eq. (37) gives $\eta=4.0\pm0.1$ ($=2.83\pm0.07$ in the reduced units of Edberg, Morriss, and Evans [24]) which is the right order of magnitude for the shear viscosity at a density close to that used by Edberg,

Morriss, and Evans (our mean translational temperature of 1.69 is somewhat higher than their value of 0.97).

Like the angular velocity profiles, we expect the translational velocity to be linearly dependent on the magnitude of the external field. To test this assumption, we have plotted in Fig. 7 $[u_x(y) - b]/F_e$ against y. The parameter b is the constant term which appears in the least squares fit of the streaming velocity to a two parameter quadratic equation and is dependent on the boundary conditions. Data are plotted for the two different values of the external field, $F_e = 0.2$ and $F_e = 0.5$. From Fig. 7 we see that both normalized functions are superimposable, confirming our expectation that translational velocity is linearly dependent on the magnitude of the external field for low values of that field.

IV. CONCLUSION

Using nonequilibrium molecular dynamics techniques, we have investigated the property of molecular spin (microrotation) in a fluid composed of diatomic molecules undergoing planar Poiseuille flow. Our simulations were performed at two different values of an effective pressure gradient and at a pore width of 10.2 molecular diameters.

We have compared the angular velocity and translational streaming velocity profiles from our work with the predictions of Navier-Stokes hydrodynamics for systems that possess spin. We find that the angular velocity profile is in general agreement with the profile predicted from the Navier-Stokes theory except for some features close to the walls which are likely to be a result of molecular packing. The angular velocity profiles scale linearly with pressure gradient.

The translational velocity profiles show almost classical behavior towards the center of the pore while at the extremities, severe slip is characterized by a sharp drop in the velocities. These profiles again scale linearly with the pressure gradient, at least in the portion that is quadratic.

The velocity profiles are discussed in terms of a dimensionless Navier-Stokes parameter, Kh, which depends on the shear, vortex and spin viscosities as well as the pore separation. The magnitude of this parameter controls the deviation from linearity of the angular velocity profile and the deviation from quadratic behavior in the translational velocity profile. From our simulations we find that Kh is of the order of 40 in reduced units.

ACKNOWLEDGMENT

[1] P. G. de Gennes, *The Physics of Liquid Crystals* (Oxford Science, Oxford, 1974).

[2] D. Forster, *Hydrodynamic Fluctuations, Broken Symmetry, and Correlation Functions* (W. A. Benjamin, Reading, Massachusetts, 1975).

[3] S. Sarman and D. J. Evans, J. Chem. Phys. **99**, 9021 (1993).

[4] H. Grad, Commun. Pure App. Math. **5**, 455 (1952).

[5] R. F. Snider and K. S. Lewchuk, J. Chem. Phys. **46**, 3163 (1967).

[6] I. Bitsanis, J. J. Magda, M. Tirrell, and H. T. Davis, J. Chem. Phys. **87**, 1733 (1987).

[7] M. Schoen, J. H. Cushman, D. J. Diestler, and J. C. L. Rhykerd, J. Chem. Phys. **88**, 1394 (1988).

[8] I. Bitsanis, S. A. Somers, H. T. Davis, and M. Tirrell, J. Chem. Phys. **93**, 3427 (1990).

[9] P. A. Thompson and M. O. Robbins, Phys. Rev. A **41**, 6830 (1990).

[10] M. Lupkowski and F. v. Swol, J. Chem. Phys. **93**, 737 (1990).

[11] S. Y. Liem, D. Brown, and J. H. R. Clarke, Phys. Rev. A **45**, 3706 (1992).

[12] J. G. Powles, S. Murad, and P. V. Ravi, Chem. Phys. Lett. **188**, 21 (1992).

[13] B. D. Todd, D. J. Evans, and P. J. Daivis, Phys. Rev. E **52**, 1627 (1995).

[14] B. D. Todd, P. J. Daivis, and D. J. Evans, Phys. Rev. E **51**, 4362 (1995).

[15] B. D. Todd and D. J. Evans, J. Chem. Phys. **103**, 9804 (1995).

[16] P. Padilla and S. Toxvaerd, J. Chem. Phys. **101**, 1490 (1994).

[17] P. Padilla, J. Chem. Phys. **103**, 2157 (1995).

[18] G. H. Peters and D. J. Tildesley, Phys. Rev. E **52**, 1882 (1995).

[19] D. J. Evans and W. B. Streett, Mol. Phys. **36**, 161 (1978).

[20] D. J. Evans and G. P. Morriss, *Statistical Mechanics of Nonequilibrium Liquids* (Academic, London, 1990).

[21] J. I. McKechnie, D. Brown, and J. H. R. Clarke, Macromolecules **25**, 1562 (1992).

[22] P. J. Daivis, K. P. Travis, and B. Todd, J. Chem. Phys. **104**, 9651 (1996).

[23] A. C. Eringen, *Contributions to Mechanics* (Pergamon, New York 1969).

[24] R. Edberg, G. P. Morriss, and D. J. Evans, Mol. Phys. **62**, 1357 (1987).